Brain Struct Funct
DOI 10.1007/s00429-014-0939-x

ORIGINAL ARTICLE

Morphology and dendritic maturation of developing principal neurons in the rat basolateral amygdala

Steven J. Ryan · David E. Ehrlich · Donald G. Rainnie

Received: 21 March 2014 / Accepted: 1 November 2014

Abstract The basolateral nucleus of the amygdala (BLA) assigns emotional valence to sensory stimuli, and many amygdala-dependent behaviors undergo marked development during postnatal life. We recently showed principal neurons in the rat BLA undergo dramatic changes to their electrophysiological properties during the first postnatal month, but no study to date has thoroughly characterized changes to morphology or gene expression that may underlie the functional development of this neuronal population. We addressed this knowledge gap with reconstructions of biocytin-filled principal neurons in the rat BLA at postnatal days 7 (P7), 14, 21, 28, and 60. BLA principal neurons underwent a number of morphological changes, including a twofold increase in soma volume from P7 to P21. Dendritic arbors expanded significantly during the first postnatal month and achieved a mature distribution around P28, in terms of total dendritic length and distance from soma. The number of primary dendrites and branch points were consistent with age, but branch points were found farther from the soma in older animals. Dendrites of BLA principal neurons at P7 had few spines, and spine density increased nearly fivefold by P21. Given the concurrent increase in dendritic material, P60 neurons had approximately 17 times as many total spines as P7 neurons. Together, these developmental transitions in BLA principal neuron morphology help explain a number of concomitant electrophysiological changes during a critical period in amygdala development.

Keywords Basal amygdala · Pyramidal · Dendritic spine · Sholl analysis

Introduction

The basolateral nucleus of the amygdala (BLA) is critical for the production of appropriate emotional responses and the processing of emotional memories (Davis et al. 2003; LeDoux 2007; Pape and Pare 2010; Stuber et al. 2011). In recent years, many studies have implicated amygdala dysfunction in the etiology of psychiatric disorders, including anxiety, depression, and autism (Adolphs et al. 2002; Rainnie et al. 2004; Shekhar et al. 2005; Truitt et al. 2007; Koob and Volkow 2010). These and other psychiatric disorders have roots in development, with early ages of onset or vulnerability to risk factors early in life (Pine et al. 1998; Kim-Cohen et al. 2003; McEwen 2003; Steinberg 2005). Furthermore, a wealth of studies have identified deficits or changes to fear learning and expression during postnatal development (Rudy et al. 1993; Sullivan et al. 2000; Wiedenmayer and Barr 2001; Hubbard et al. 2004; Kim and Richardson 2008; Ito et al. 2009; Raineki et al. 2009; Pattwell et al. 2011, 2012). Despite the critical role for the amygdala in the expression of normative and maladaptive emotional behaviors, relatively few studies have characterized how BLA structure and function change with age.

Many prior studies addressing maturation of the BLA have been performed in rats. These studies have identified a window during the first postnatal month wherein the morphology and physiology of the nucleus undergo rapid and pronounced change. In particular, during this window

S. J. Ryan and D. E Ehrlich contributed equally.

S. J. Ryan · D. E. Ehrlich · D. G. Rainnie (✉)
Department of Psychiatry and Behavioral Sciences, Division of Behavioral Neuroscience and Psychiatric Disorders, Yerkes Research Center, Emory University School of Medicine, 954 Gatewood Rd., Atlanta, GA 30033, USA
e-mail: drainni@emory.edu

Published online: 09 November 2014

the volume of the BLA increases while the density of neurons is reduced by half (Morys et al. 1998; Rubinow et al. 2009; Chareyron et al. 2012). Neurons in the BLA grow during this period, with somas and dendritic arbors expanding (Escobar and Salas 1993). We recently characterized the developmental changes to electrophysiological properties of BLA principal neurons, which comprise approximately 85 % of BLA neurons and mediate virtually all output of the nucleus (Ehrlich et al. 2012). Specifically, we showed that BLA principal neurons exhibit significant changes to their excitability and sensitivity to synaptic input across the first postnatal month, including a tenfold reduction in input resistance and a hyperpolarization of action potential threshold greater than 5 mV. There are also concomitant changes to the waveform and patterning of action potential output, including the emergence of a fast after-hyperpolarization and spike doublets.

While previous studies have addressed gross morphological changes to the BLA and its component neurons throughout postnatal development, several important knowledge gaps remain. The only study to date examining the morphology of individual neurons in the BLA was not specific to principal neurons and did not address features such as the quantity or branching of dendritic material or the expression of spines (Escobar and Salas 1993). Developmental changes to these features should substantially alter neuronal function, as the surface area of BLA principal neurons and the types of ion channels inserted into their membranes directly impact neurophysiology, including firing patterns (Mainen and Sejnowski 1996). We have addressed this knowledge gap by characterizing BLA principal neuron morphology throughout the first postnatal month and in adulthood. Specifically, we used whole-cell patch clamp at postnatal days 7, 14, 21, 28, and 60 to fill neurons with biocytin for post hoc morphological reconstruction and analysis. Here, we describe a number of changes to the soma, dendritic arbor, and dendritic spines of developing BLA principal neurons.

Materials and methods

Ethical approval

All experimental protocols strictly conform to National Institutes of Health guidelines for the Care and Use of Laboratory Animals, and were approved by the Institutional Animal Care and Use Committee of Emory University.

Animals

Male rats born in-house to outbred, time-mated Sprague–Dawley female rats (embryonic day 5 on arrival from Charles River, Wilmington, MA, USA) were used in all experiments. Pups were housed with the dam prior to weaning on postnatal day (P)22 or P23 (considering P1 as day of birth). After weaning, rats were isolated by sex and housed three to four per cage with access to food and water ad libitum. Animals attributed to each developmental time-point (P7, P14, P21, P28, and P60) were used on that day or the following day (P7–8, P14–15, P21–22, P28–29, and P60–61, respectively).

Slice physiology

To enable neuronal reconstructions at each time-point, we performed whole-cell patch clamp to identify BLA principal neurons based on electrophysiological properties as described previously (Ehrlich et al. 2012) and to visualize neurons, biocytin (0.35 %, Sigma-Aldrich, St Louis, MO, USA) was included in the patch recording solution. Acute brain slices containing the BLA were obtained as previously described (Rainnie 1999). Briefly, animals were decapitated under isoflurane anesthesia (Fisher Scientific, Hanoverpark, IL, USA) if P11 or older and without anesthesia if younger. Then the brains were rapidly removed and immersed in ice cold, 95 % oxygen–5 % carbon dioxide-perfused 'cutting solution' with the following composition (in mM): NaCl (130), $NaHCO_3$ (30), KCl (3.50), KH_2PO4 (1.10), $MgCl_2$ (6.0), $CaCl_2$ (1.0), glucose (10), ascorbate (0.4), thiourea (0.8), sodium pyruvate (2.0), and kynurenic acid (2.0). Due to changes in tissue consistency, coronal slices containing the BLA were cut at a thickness of 300 μm at P7 and P14 or 350 μm from P21 onwards. Slices were prepared using a Leica VTS-1000 vibrating-blade microtome (Leica Microsystems Inc., Bannockburn, IL, USA). Slices were kept in oxygenated cutting solution at 32 °C for 1 h before transferring to regular artificial cerebrospinal fluid (ACSF) containing (in mM): NaCl (130), $NaHCO_3$ (30), KCl (3.50), KH_2PO_4 (1.10), $MgCl_2$ (1.30), $CaCl_2$ (2.50), glucose (10), ascorbate (0.4), thiourea (0.8) and sodium pyruvate (2.0).

Patch clamp recording

Individual slices were transferred to a recording chamber mounted on the fixed stage of a Leica DMLFS microscope (Leica Microsystems Inc., Bannockburn, IL, USA) and maintained fully submerged and continuously perfused with oxygenated 32 °C ACSF at a flow rate of 1–2 mL min^{-1}. The BLA was identified under 10 × magnification. Individual BLA neurons were identified at 40x using differential interference contrast (DIC) optics and infrared (IR) illumination with an IR-sensitive CCD camera (Orca ER, Hamamatsu, Tokyo Japan). The location of recorded neurons was chosen randomly

throughout the BLA. Putative principal neurons were selected based on soma size, and their identities were later verified electrophysiologically, as described below. Patch pipettes were pulled from borosilicate glass and had a resistance of 4–6 MΩ. Patch electrode solution had the following composition (in mM): potassium gluconate (130), KCl (2), HEPES (10), $MgCl_2$ (3), K-ATP (2), Na-GTP (0.2), phosphocreatine (5), and 0.35 % biocytin, titrated to pH 7.3 with KOH, and 290 mosmol L^{-1}. Data acquisition was performed using either a MultiClamp 700A or an Axopatch 1D amplifier in conjunction with pCLAMP 10.2 software and a DigiData 1322A AD/DA interface (Molecular Devices, Sunnyvale, CA, USA). Whole-cell patch clamp recordings were obtained and low-pass filtered at 2 kHz and digitized at 10 kHz. The membrane potential was held at −60 mV for all neurons if not specified. Cells were excluded if they did not meet the following criteria: a stable resting membrane potential more negative than −55 mV; access resistance lower than 30 MΩ; stable access resistance throughout recording, changing less than 15 %; and action potentials crossing 0 mV. BLA principal neurons were distinguished from interneurons, as previously, by their input resistance and spiking pattern in response to injection of a series of 10 hyperpolarizing and depolarizing, 1 s long, square-wave current steps (Ehrlich et al. 2012; Rainnie et al. 2006). Current amplitudes were scaled so that, for each cell, the peak voltage deflections were approximately − 80 mV and − 40 mV. Traces were analyzed using Clampfit 10.2 (Molecular Devices, Sunnyvale, CA, USA).

Histochemical processing

Patched neurons were labeled with biocytin (Sigma-Aldrich, St Louis, MO, USA) included in the patch pipette recording solution. After neurons were recorded for at least 15 min, slices were fixed in 10 % buffered formalin (Fisher Scientific, Hanoverpark, IL, USA) for 12–72 h, and then transferred to cryoprotectant for storage at −20 C. After three consecutive 10 min washes in 0.05 M phosphate buffered saline (PBS), slices were permeabilized for 30 min in phosphate buffered saline (PBS) and 0.5 % Triton X-100 (Sigma-Aldrich, St Louis, MO, USA). Slices were then treated with Alexa Fluor 488-conjugated Streptavidin (Invitrogen, Grand Island, New York, USA) diluted to 1:1,000 in PBS with Triton X-100 overnight at room temperature. Slices were then washed 2 times for 1 h each in 0.05 M PBS and washed for 10 min in 0.05 M phosphate buffer. Finally, the slices were mounted on glass slides, air dried for 2–12 h, and cover-slipped with mowiol mounting medium (Sigma-Aldrich, St Louis, MO, USA). To create representative outlines of the nucleus at different positions along the rostrocaudal axis for depicting the location of recorded neurons, one rat at each juvenile timepoint was transcardially perfused and the BLA was traced in every sixth section of thickness 60 μm (P14, P21, and P28) or 90 μm (P7). The locations of neuron reconstructions were registered to these outlines using soma location, excluding two neurons for which location could not be recovered. The BLA was identified by its location between the external capsule and longitudinal association bundle. Reconstructions were performed only for neurons with somas located in the ventral half of the basolateral complex, because the border between the BLA and the lateral nucleus (located dorsally) is poorly defined in the immature brain. Similarly, there is no precedent for distinguishing the anterior and posterior subdivisions of the immature BLA, so neurons were grouped based on location in the anterior or posterior half of the nucleus.

Neuronal reconstruction and data Analysis

For morphological analysis, the dendritic arbor of each neuron was first reconstructed by hand using Neurolucida neuron tracing software (MicroBrightField, Colchester, VT) from single z-stack images taken at 10x magnification with a 0.4 μm step size using a Leica DM5500B spinning disk confocal microscope (Leica Microsystems Inc., Bannockburn, IL, USA) and SimplePCI data acquisition software (Compix, Sewickley, PA). Slices were examined live at 63 × to support tracing of fine or overlapping dendritic segments. Reconstructions of neuronal somas were performed using AutoNeuron workflow in Neurolucida from image stacks obtained with a 63 × objective. Quantitative analysis of reconstructions was performed using Neurolucida Explorer (MicroBrightField). The volume and surface area of somas were estimated using the 'Marker and Region Analysis' subroutine to provide a 3-D contour summary. Dendritic length and branching were analyzed in Neurolucida Explorer using Sholl analyses with ring radius increments of 2 μm, and data were analyzed in Matlab (The MathWorks, Natick, MA, USA). Corrections were made for shrinkage due to tissue processing. Thickness of processed tissue samples was estimated using confocal microscopy and compared to known thickness of live samples before fixation and mounting. Tissue correction factors varied between 2.8 and 4.6, and there was no clear relationship between postnatal age and the degree of shrinkage.

To estimate the average spine density for BLA principal neurons, we manually counted dendritic spines with Neurolucida on image stacks of dendrite segments taken at 100 × magnification. The sampling method is explained in Fig. 1. For each neuron, spines were counted by a blinded experimenter on 10 non-overlapping dendritic segments. Each segment spanned 50 μm and was centered on 1 of 10 points in the dendritic arbor chosen pseudo-randomly by a

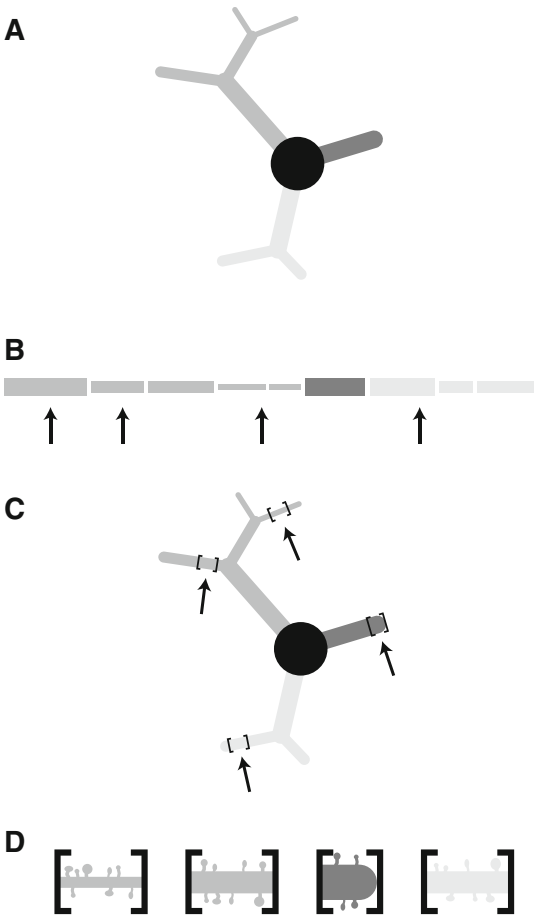

Fig. 1 Spine counting methodology is depicted for a cartoon neuron (**a**), comprised of a soma and three dendritic branches. **b** Locations for spine counting are randomly selected throughout the arbor (see "Materials and methods"). **c** Segments spanning up to 50 µm, centered on the randomly chosen locations, are imaged at × 100 magnification and **d** spines are counted manually. Average spine density is calculated for each segment and averaged across these locations to determine the average density for each neuron

custom Matlab script (available upon request), making the selections agnostic to branch order or distance from soma. This script weighted each micron-long section of the dendrite evenly when making selections, so the distribution of sampled segments reflected the actual distribution of dendritic material with regard to branch order and primary dendrite. All protrusions were counted as spines. Total spine number was estimated for each neuron individually using the product of average spine density and aggregate dendritic length, defined as the sum of the lengths of all dendritic segments.

Statistics

Unless otherwise noted, data are presented as mean ± SEM. To compensate for age-dependent changes in variance (assessed using Bartlett's test with GraphPad, GraphPad Software Inc., La Jolla, CA, USA), data for soma volume, critical value of dendritic length, dendritic spine density, and total spine estimate were log transformed before statistical analysis. The values for aggregate dendritic length, critical value of dendritic length, dendritic spine density, and total dendritic spine estimate were fit with a Boltzman sigmoidal equation (Eq. 1) in GraphPad. The inflection point of the curve occurs at $x = V_{1/2}$ and with a slope of α. A_2 and A_1 reflect the lower and upper asymptotes, respectively. Unless otherwise noted, data sets were analyzed with a One-way ANOVA to determine effects of age (GraphPad). Data from Sholl analyses were analyzed with Two-way ANOVA to determine effects of age and distance from soma. Data for aggregate dendritic length, branch point number, and spine density were compared across anterior and posterior BLA subdivisions using Two-way ANOVAs (factors of subdivision and age). Posthoc tests were applied only following significant main effects in ANOVA. Tukey's tests were used for posthoc comparisons in all experiments but one, because of limited a priori knowledge regarding developmental trajectories. For the experiment presented in Fig. 6d comparing dendritic material at specific distances from the soma, Bonferroni corrections were applied to contrasts at select intervals of distances to limit the number of total comparisons.

$$y = A_2 + (A_1 - A_2)/(1 + e^{(V_{1/2} - x)/\alpha}) \quad (1)$$

Results

In total, 40 BLA principal neurons were filled with biocytin and reconstructed at postnatal day 7 (P7), P14, P21, P28, and P60 ($n = 8$ per time-point). Basic electrophysiological properties were measured and found to be consistent with previously reported values (Fig. 2; Ehrlich et al. 2012). Specifically, neurons at P7 and P14 were highly sensitive to direct current injection, reflecting large input resistances, but fired action potentials at lower frequencies than more mature neurons (Fig. 2a). Action potentials had larger amplitudes and shorter durations with age, as action potential threshold became more hyperpolarized (Fig. 2b). In addition, immature neurons charged more slowly in response to hyperpolarizing current injections (Fig. 2c).

Following recordings, filled neurons were stained and visualized post hoc to make reconstructions (see "Materials and methods"). Representative photomicrographs are provided at each time-point (Fig. 3a). The locations of reconstructed neurons are illustrated in Fig. 3b. To compare dendritic arborization across age, representative neuronal reconstructions are depicted for each time-point in Fig. 4. We observed a variety of developmental changes to BLA principal neuron morphology that are quantified in detail below. Principal neurons at all ages lacked a consistent orientation in the slice.

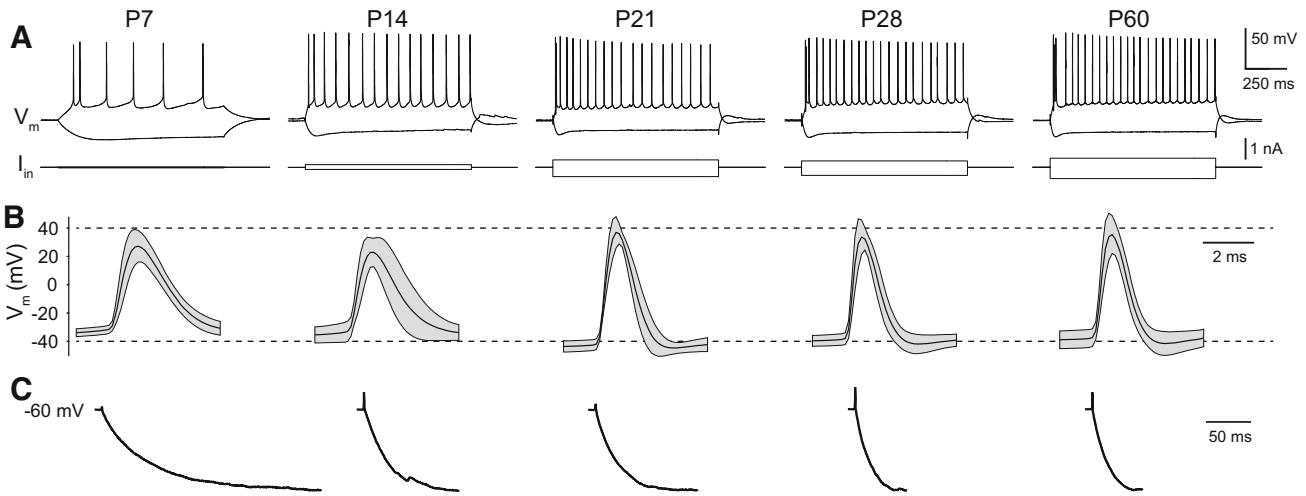

Fig. 2 BLA principal neuron electrophysiology matures in parallel with morphology. Whole-cell patch clamp recordings were used to fill BLA principal neurons with biocytin. (**a**) Representative responses of developing neurons to depolarizing and hyperpolarizing current injections from holding potential of −60 mV. Current injections were varied with age to elicit consistent voltage deflections, given the nearly tenfold decrease in input resistance from P7 to P60 (Ehrlich et al. 2012). **b** Action potential waveform (mean as *black line*, standard deviation as *gray band*) of developing neurons included in this study. **c** Charging curves in response to hyperpolarizing current injection, averaged across neurons and normalized across time-points

Soma size

We first quantified somatic volume and surface area of BLA principal neurons throughout postnatal development (Fig. 5). Somatic diameters ranged between 10 and 16 μm and somatic volume changed significantly during postnatal development (Fig. 5a, $P < 0.001$, One-way ANOVA, $F_{4,29} = 6.51$), increasing across the first three postnatal weeks and then remaining stable until P60. Mean somatic volume increased by 66 % from P7 to P21, followed by a change of less than 3 % by P60. Somatic volume exhibited an asymptotic relationship with age, increasing from 2,644 ± 186.7 μm^3 (mean ± SEM) at P7 ($n = 7$) to 3,758 ± 176.5 μm^3 at P14 ($n = 7$; Tukey's post hoc test, $P > 0.05$), 4,399 ± 444.9 μm^3 at P21 ($n = 7$, $P < 0.01$), 4,250 ± 174.1 μm^3 at P28 ($n = 6$, $P < 0.01$), and 4,304 ± 471.9 μm^3 ($n = 7$) by P60.

A qualitatively similar but non-significant trajectory was exhibited by somatic surface area (Fig. 5b, $P > 0.05$, One-way ANOVA, $F_{4,29} = 2.146$). Somatic surface area increased from 1,106 ± 68.2 μm^2 at P7 ($n = 7$) to 1,276 ± 60.4 μm^2 at P14 ($n = 7$), 1,327 ± 116 μm^2 at P21 ($n = 7$), 1,395 ± 54.6 μm^2 at P28 ($n = 6$), and 1,495 ± 150.9 μm^2 at P60.

Growth and subsequent retraction of dendritic arbor

Extensive remodeling of dendritic architecture of BLA principal neurons also occurred across postnatal development (Fig. 6). The aggregate length of dendrites for each neuron changed significantly with age ($P < 0.0,001$, One-way ANOVA, $F_{4,34} = 26.41$), increasing more than threefold across the first postnatal month (Fig. 6a). Aggregate dendritic length increased significantly from 2.347 ± 0.184 mm at P7 ($n = 7$) to 5.417 ± 0.474 mm at P14 ($n = 8$; Tukey's post hoc test, $P < 0.001$), 6.665 ± 0.379 mm at P21 ($n = 8$; $P < 0.001$), 7.709 ± 0.432 mm at P28 ($n = 8$; $P < 0.001$), and 7.908 ± 0.540 mm at P60 ($n = 8$; $P < 0.001$). The aggregate dendritic length also increased significantly from P14 to P28 ($P < 0.01$). The distribution of aggregate dendritic length vs. Age was fit with a sigmoidal Boltzmann function (Eq. 1), which estimated the inflection point at $V_{1/2}$ - = 10.72 days with a slope of $\alpha = 4.90$ days. The lower asymptote of aggregate length was constrained to be greater than or equal to 0, and was estimated to be $A_2 = 0.0$ μm and the upper asymptote to be $A_1 = 7{,}837$ μm. The goodness of fit was $R^2 = 0.749$. No difference in aggregate dendritic length was found between anterior and posterior subdivisions of the BLA (Two-way ANOVA, main effect of subdivision: $F_{1,26} = 0.59$, $P = 0.45$).

The observed increase in aggregate dendritic length with age corresponded with an increased distance of that material to the soma (Fig. 6b). Using a Sholl analysis with concentric rings of 4 μm thickness, we were able to determine the critical value for dendritic length, defined as the radius of the Sholl ring with the greatest amount of dendritic length. With age, dendrites became concentrated farther from the soma, with the critical value increasing significantly across the first postnatal month ($P < 0.0001$,

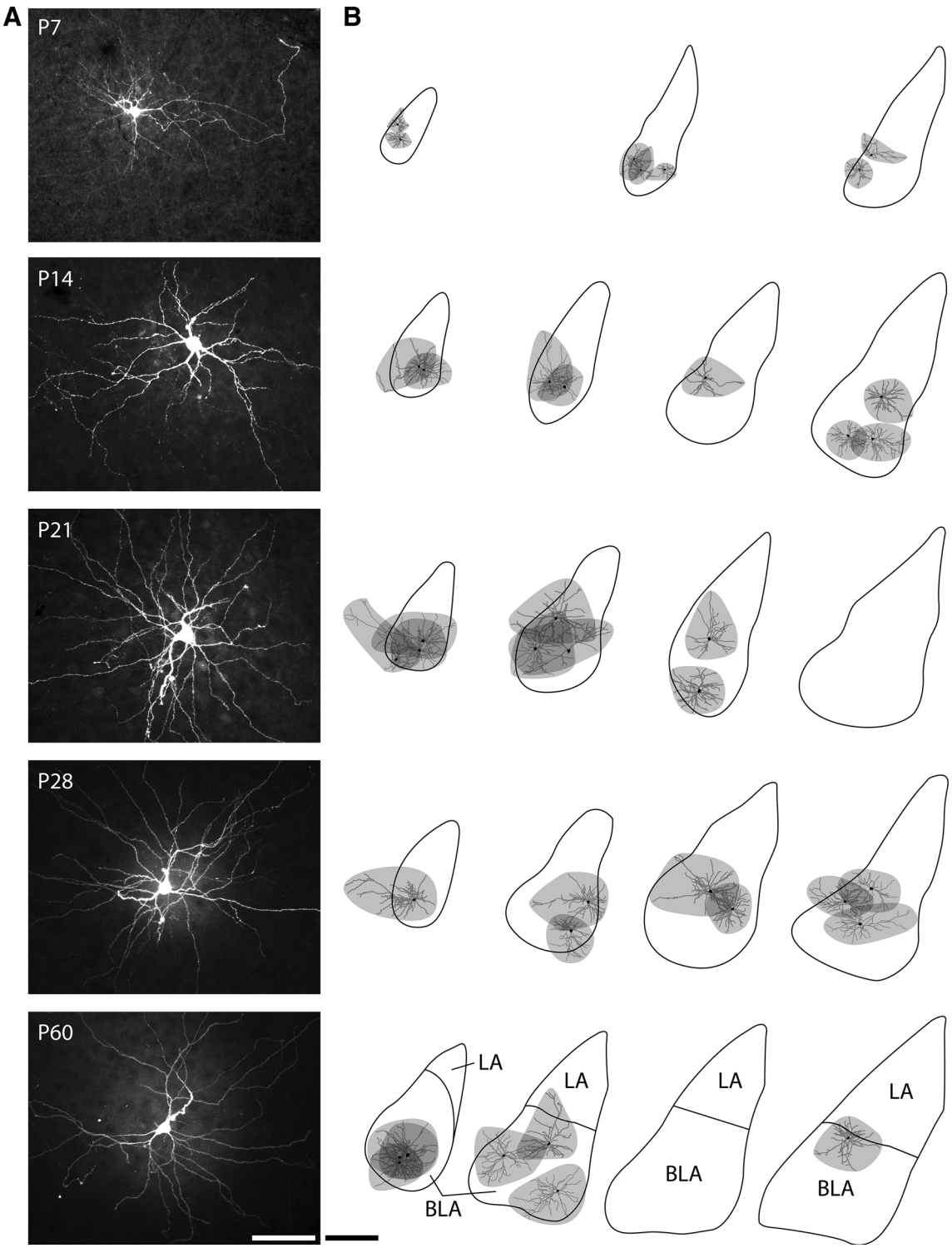

Fig. 3 Location of reconstructed BLA principal neurons. **a** Representative photomicrographs of filled neurons at each time-point were produced from maximum projections of z-stack images through entire recording slices. *Scale bar* represents 100 μm. **b** Approximate locations and dendritic arborization of filled BLA neurons at each time-point are depicted on outlines of the basolateral complex from representative coronal sections. Soma and dendrites of reconstructed neurons (from slices of 300–350 μm thickness) are illustrated in *black* and *gray*, respectively, while the area covered by the dendritic arbor is shaded in gray. Outlines of the basolateral complex were drawn from every sixth section of 90 μm (P7) or 60 μm thickness (P14–P28). Outlines of the BLA and the lateral nucleus (LA) at P60 correspond to Bregma coordinates −2.30, −2.80, −3.14, and −3.30 mm (Paxinos and Watson 1997). *Scale bar* represents 500 μm

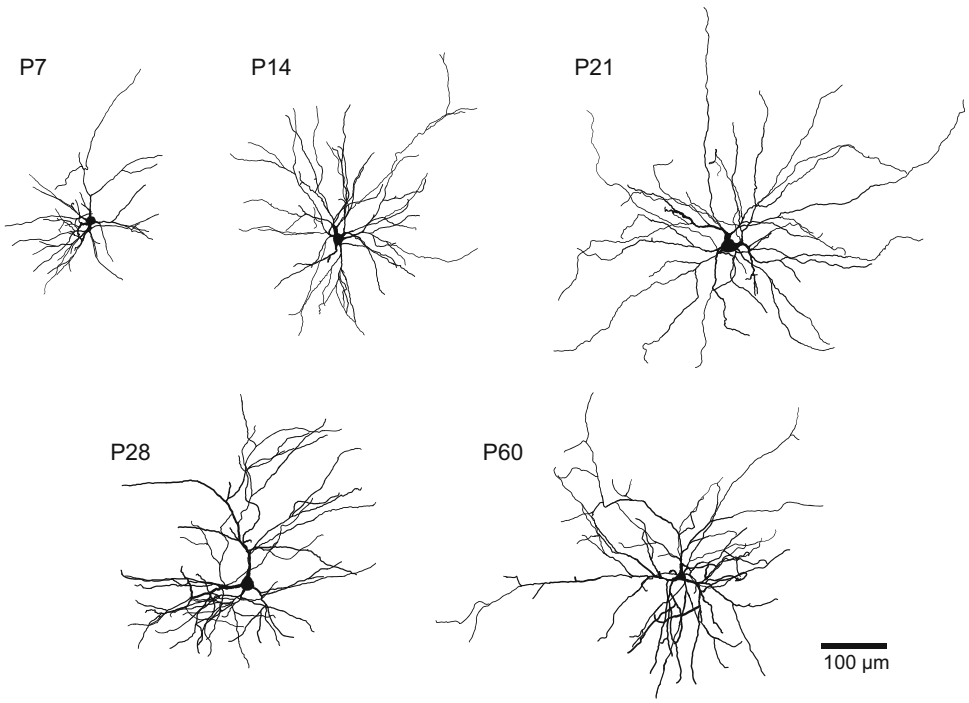

Fig. 4 Soma and dendrites of BLA principal neurons grow during the first postnatal month. Reconstructions of representative, biocytin-filled BLA principal neurons at postnatal days 7 (P7), 14, 21, 28, and 60

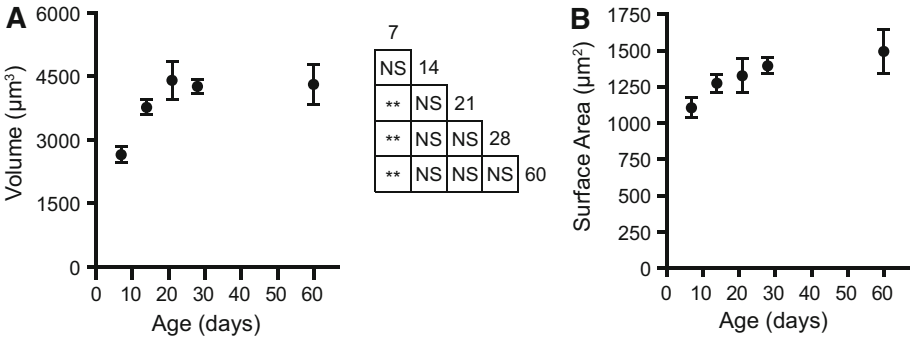

Fig. 5 Soma size increases across the first postnatal month. Soma volume (**a**) and surface area (**b**) of BLA principal neurons are depicted as mean ± SEM at postnatal days 7 (P7), 14, 21 and 28. At P7, P14, P21 and P60, $n = 7$; at P28, $n = 6$. The results of Tukey's tests following one-way ANOVA are depicted in an inset grid (* $P < 0.05$; ** $P < 0.01$; *** $P < 0.001$; *NS* not significant)

One-way ANOVA, $F_{4,35} = 11.96$). Specifically, the critical value for dendritic length increased significantly from 41.0 ± 5.1 µm at P7 ($n = 8$; Tukey's post hoc test, $P < 0.01$) to 73.0 ± 4.8 µm at P14 ($n = 8$) and increased to 87.5 ± 10.7 µm at P21 ($n = 7$, $P < 0.001$ vs P7), 98.0 ± 6.5 µm at P28 ($n = 8$; $P < 0.001$), and 123.0 ± 13.5 µm at P60 ($n = 8$; $P < 0.001$).

The proximity of dendrites to the soma matures in a specific pattern, exemplified by the representative reconstructions in Fig. 4. Across the first few postnatal weeks, dendrites extend farther from the soma. From P21 to P28 there is expansion of dendrites near the soma, and by P60 there is a reduction of dendrites proximal to the soma and an expansion of the more distal branches. Using Sholl analysis, we identified specific portions of the dendritic arbor where significant growth and retraction occur during postnatal development (Fig. 6d; Two-way ANOVA with Bonferroni post hoc tests; main effect of age: $P < 0.0001$, $F_{4,1155} = 112.7$ greater than or equal to soma: $P < 0.0001$, $F_{34,1155} = 219.9$; interaction effect: $P < 0.0001$, $F_{136,1155} = 9.478$). In P7 neurons ($n = 7$), more than 98 % of dendritic length is found within 200 µm of the soma. By P14, the proportion found within 200 µm drops to 91.6 %, while 99.8 % of dendritic length is found within 400 µm of the soma. From P7 to P14, there is also a significant expansion of dendrites in the region 40–180 µm from the soma ($P < 0.01$). By P21, only 96.8 % of dendritic material is found within 400 µm of the soma, with the remainder extending as far as 640 µm from the soma. From P14 to P21, significant growth of dendrites occurs in the

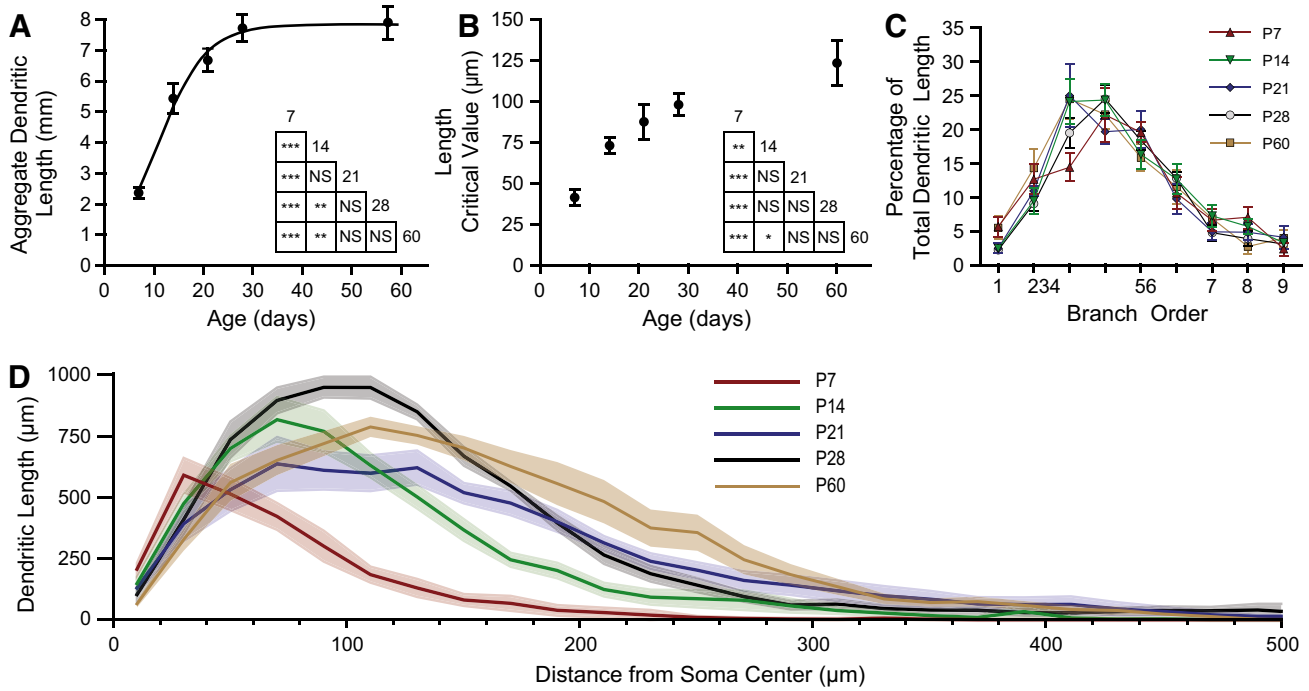

Fig. 6 Dendritic arbors expand with a specific pattern across postnatal development. Sholl analysis was performed on reconstructed neurons with 20 µm steps between rings. Aggregate length (**a**) and the critical value for length (**b**) of the dendritic arbor are plotted versus age as mean ± SEM, with a best-fit sigmoidal Boltzmann curve. The results of Tukey's tests following two-way ANOVA are depicted in inset grids (* $P < 0.05$; ** $P < 0.01$; *** $P < 0.001$; *NS* not significant; $n = 8$ per time-point). **c** Percentage of total dendritic length found in branches of a given order is plotted as mean ± SEM for each age ($n = 8$ neurons per age). **d** The profile of dendritic length derived from the Sholl analysis is plotted as mean (*black line*) and SEM (*grey band*) versus distance from the center of the soma, illustrating the expansion and pruning of the dendritic arbor with age ($n = 8$)

region 160–200 µm from the soma ($P < 0.01$). At P28, dendritic arbors occupy a similar space as those at P21, extending as far as 660 µm from the soma, with 96.9 % of dendritic length found within 400 µm of the soma. From P21 to P28, there was a significant increase in dendritic material found in the region 40–120 µm from the soma ($P < 0.001$). The developmental expansion of dendrites in this window is reversed by P60, at which age significantly less dendritic material is found in the region 40–100 µm from the soma ($P < 0.05$ vs. P28). By P60, the reduction in dendritic length also occurs in the most distal parts of the arbor, with 99.1 % of dendritic length being found within 400 µm of the soma (compared to 96.9 % at P28).

We also examined the pattern of dendrite maturation by considering the growth of specific orders of dendritic branches (Fig. 6c). When we normalized the dendritic length for individual orders of branches to the aggregate dendritic length of an entire neuron, we found the majority of dendritic length in second through sixth order dendrites. The length of dendrites varied significantly by branch order, but age did not significantly affect this distribution (Two-way ANOVA; main effect of branch order: $P < 0.0001$, $F_{8,268} = 54.58$; main effect of age: $P > 0.05$, $F_{4,268} = 0.26$).

Maturation of dendritic branching

We also investigated the maturation of branch points in the dendritic arbor, because the location of branch points determines the relationship between dendrite order and proximity to the soma (Fig. 7). The number of primary dendrites was consistent throughout postnatal development (Fig. 7a; $P > 0.05$, Kruskal–Wallis, $H(4) = 5.93$; mean ± SD: 7 ± 2.4 at P7, 5.75 ± 1.5 at P14, 5.5 ± 1.1 at P21, 6.1 ± 1.5 at P28, and 7.75 ± 2.4 at P60; $n = 8$). We analyzed the total number of branch points in the dendritic arbor for neurons at each time-point, and found no significant effect of age (Fig. 7b; $P > 0.05$, Kruskal–Wallis, $H(4) = 7.10$; mean ± SD: 42 ± 18.0 at P7, 34.7 ± 13.3 at P14, 35.0 ± 8.5 at P21, 45.0 ± 8.8 at P28, and 34.5 ± 8.8 at P60; $n = 7$–8). No difference in branch point number was found between anterior and posterior subdivisions of the BLA (Two-way ANOVA, main effect of subdivision: $F_{1,26} = 2.36$, $P = 0.14$).

Furthermore, we quantified the proximity of branch points to the soma using a Sholl analysis with 40 µm thick rings. We found significant changes in the proximity of branch points to the soma with age (Fig. 7c; Two-way ANOVA with Tukey's post hoc tests; main effect of

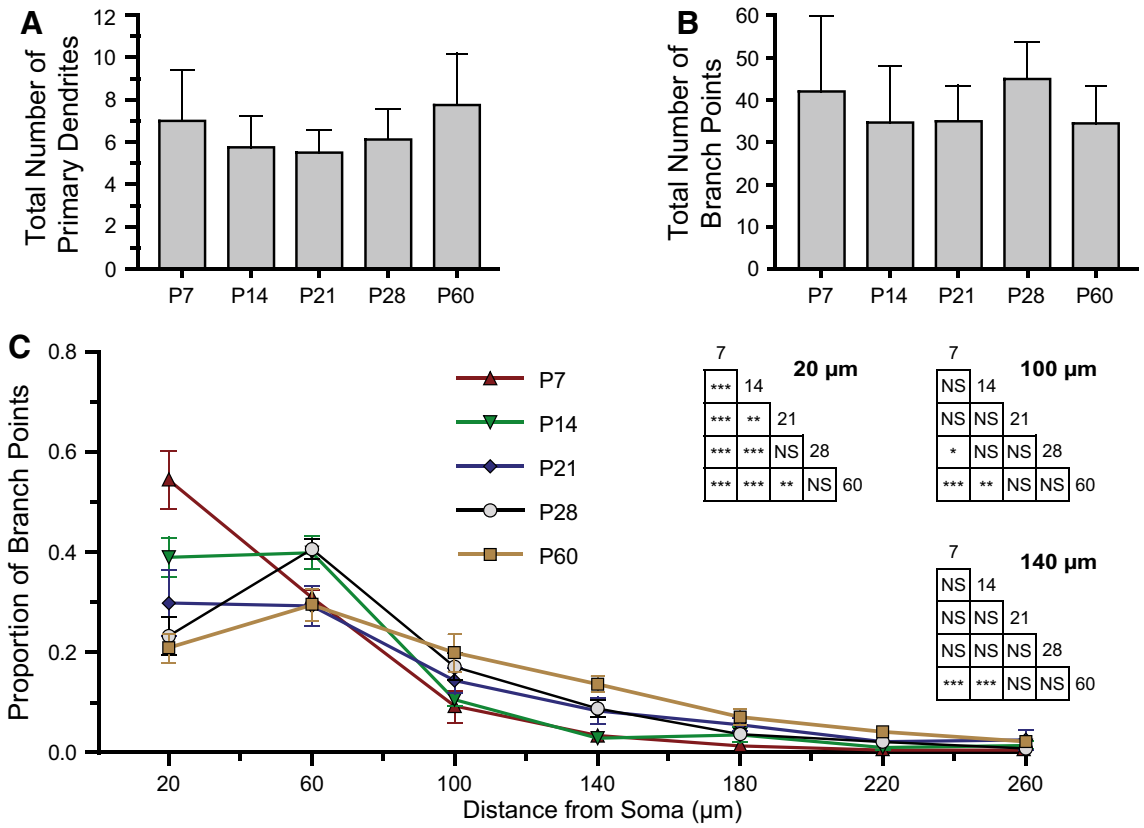

Fig. 7 Dendritic branch points become more distant from the soma during postnatal development. Bar graphs illustrate the mean ± SD of the total number of primary dendrites (**a**) and branch points (**b**) for BLA principal neurons at each time-point ($n = 8$). **c** The proximity of branch points to the soma was derived from Sholl analyses on reconstructed neurons with 40 µm thick rings, and the proportion of total branch points found in each ring is plotted as mean ± SEM ($n = 8$). The results of Tukey's tests following two-way ANOVA are depicted in inset grids for Sholl rings with significant effects of age, namely those centered at 20, 100, and 140 µm from the soma (* $P < 0.05$; ** $P < 0.01$; *** $P < 0.001$; *NS* not significant)

distance from soma: $P < 0.0001$, $F_{15,512} = 220.9$; interaction of age and distance from soma: $P < 0.0001$, $F_{60,512} = 6.167$). In P7 neurons, branch points were found very close to the soma, with 54.5 ± 15 % occurring within 40 µm of the soma and 97.8 ± 4.3 % occurring within 160 µm (mean ± SEM, $n = 7$). With age, branch points transitioned away from the soma: by P14, branch points were found more distally, extending as far as 320 µm from the soma, and with significantly fewer within 40 µm (9.0 ± 10.4 %, $P < 0.001$, $n = 7$). The proportion of branch points within 40 µm of the soma also decreases significantly from P14 to P21 (29.8 ± 17 %, $P < 0.01$, $n = 7$), and from P14 to P28 (23.3 ± 10.6 %, $P < 0.001$, $n = 8$) and P60 (20.8 ± 8.2 %, $P < 0.001$, $n = 8$). Conversely, the proportion of branch points located more distally increases significantly with age. Specifically, in P7 neurons 3.3 ± 4.3 % of branch points are located 120–160 µm from the soma, while this number increases to 8.3 ± 7 % at P21 and significantly increases to 8.8 ± 4.6 % at P21 ($P < 0.001$)and 13.7 ± 4.4 % at P60 ($P < 0.001$, see Fig. 7c).

Developmental emergence of dendritic spines

We next investigated the maturation of dendritic spines (Fig. 8), which were much more apparent on the arbors of neurons at later time-points. Neurons at P7 frequently possessed smooth dendrites with few spines, while neurons at P21 and older had spine-laden dendrites (Fig. 8a). To quantify the emergence of dendritic spines with age, we counted spines on 10 random segments of dendrite for neurons at each time-point (see Methods). We found that the density of dendritic spines changed significantly with age, increasing nearly sixfold across the time period studied, reaching adult levels at the end of the first postnatal month (Fig. 8b; $P < 0.0001$, One-way ANOVA, $F_{4,25} = 59.41$; $n = 6$ neurons per time-point). Specifically, neurons at P7 had a spine density of 0.21 ± 0.03 spines/µm (mean ± SEM) which increased significantly to 0.53 ± 0.05 spines/µm at P14 ($P < 0.001$), 1.03 ± 0.12 at P21 ($P < 0.001$), 1.18 ± 0.05 at P28 ($P < 0.001$), and 1.29 ± 0.07 at P60 ($P < 0.001$). Spine density also increased significantly from P14 to all later time-points

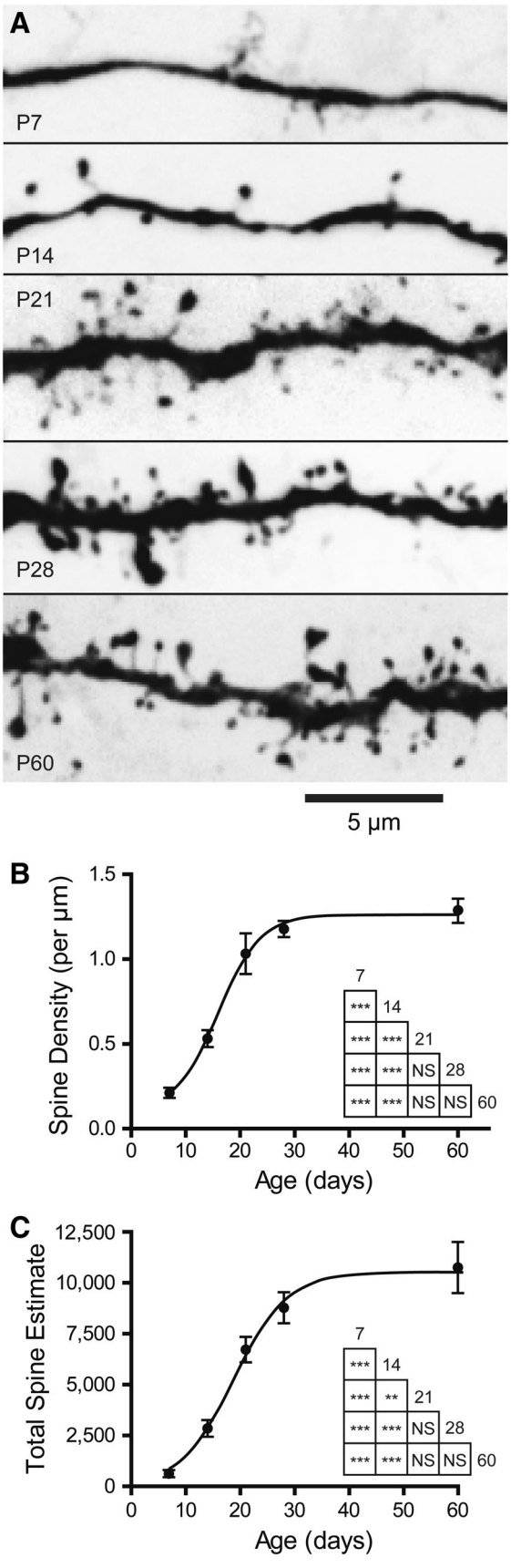

◀**Fig. 8** Dendritic spines emerge during the first month of postnatal development in BLA principal neurons. **a** Representative maximum projections of z-stack photomicrographs taken of segments of dendrites from filled BLA principal neurons at each time-point. **b**, **c** Dendritic spine density and the estimated total number of spines are plotted as mean ± SEM for neurons at each time-point ($n = 6$). The results of Tukey's tests following one-way ANOVA are depicted in inset grids (* $P < 0.05$; ** $P < 0.01$; *** $P < 0.001$; *NS* not significant)

($P < 0.001$). The distribution of dendritic spine density vs. age was fit with a sigmoidal Boltzmann function (Eq. 1), which estimated the inflection point at $V_{1/2} = 15.97$ days with a slope of $\alpha = 3.89$ days. The lower asymptote for spine density was estimated to be $A_2 = 0.10$ spines and the upper asymptote to be $A_1 = 1.26$ spines. The goodness of fit was $R^2 = 0.868$. No difference in spine density was found between anterior and posterior subdivisions of the BLA (Two-way ANOVA, main effect of subdivision: $F_{1,20} = 0.62$, $P = 0.44$).

Using our measurements of mean spine density and the aggregate dendritic length from our reconstructions, we were able to estimate the total number of dendritic spines for each neuron (Fig. 8c). These estimates suggest the total number of spines is more than seventeen times larger at P60 than at P7, as the number of spines increases significantly across postnatal development ($P < 0.0001$, One-way ANOVA, $F_{4,25} = 61.61$; $n = 6$). Specifically, neurons at P7 had an estimated 601 ± 154 spines (mean ± SEM) which increased significantly to 2,822 ± 379 spines at P14 ($P < 0.001$), 6,694 ± 572 at P21 ($P < 0.001$), 8,745 ± 698 at P28 ($P < 0.001$), and 10,719 ± 1,150 at P60 ($P < 0.001$). Total spine number also increased significantly from P14 to all later time-points ($P < 0.01$). As with spine density, the distribution of total dendritic spines vs. age was fit with a sigmoidal Boltzmann function (Eq. 1), which estimated the inflection point at $V_{1/2} = 18.8$ days with a slope of $\alpha = 4.92$ days. The lower asymptote for spine density was constrained at $A_2 = 0$ spines and the upper asymptote was estimated to be $A_1 = 10{,}520$ spines. The goodness of fit was $R^2 = 0.83$.

Discussion

In this study, we presented a detailed analysis of the morphological properties of BLA principal neurons, conducted across the first two postnatal months in rats. During this window, BLA principal neurons exhibit a variety of structural changes with the most dramatic maturation occurring before P21. Significant morphological changes included: soma size increasing nearly twofold from P7 to P28; a threefold increase in aggregate dendritic length from P7 to P21; a monotonic increase in length critical value

Table 1 Ontogeny of amygdala-related behavior in the rat

Behavior or function	Emerges	Reference(s)
Avoidance of aversively conditioned stimuli	P10	Sullivan et al. 2000
Long-term potentiation of amygdala afferents	P10	Thompson et al. 2008
Innate defensive behavior (freezing upon exposure to conspecific)	P14	Takahashi 1992
Amygdala activation upon exposure to conspecific	P12	Moriceau et al. 2004
Distinct responses to appetitive and aversive stimuli	P12	Camp and Rudy 1988
Conditioned suppression of heart rate	P16-17	Campbell and Ampuero 1985, Hunt 1999
Conditioned freezing	P16-18	Hunt et al. 1998, Barnet and Hunt 2006
Fear-potentiated startle to shock-paired tone or odor	P23-25	Hunt et al. 1994, Richardson et al. 2000, Barnet and Hunt 2006
Extinction of learned fear becomes new learning, not erasure	P23	Kim and Richardson 2007
Extinction requires NMDA receptors	P23	Langton et al. 2007
Re-extinction becomes amygdala independent	P24	Kim and Richardson 2008
Trace and long-delay fear conditioning	P28	Moye and Rudy 1987, Barnet and Hunt 2005
Fear-potentiated startle to shock-paired light	P30	Hunt et al. 1994

from P7 to P60; a shift of branch points more distally in the dendritic arbor through P60; and an increase in the density of dendritic spines, reaching maturity around P28. Taken together, these developmental changes to principal neuron morphology help explain a wealth of electrophysiological changes occurring in the first postnatal month, including dramatic changes to passive membrane properties, action potential waveform and patterning, and intrinsic frequency preference (Ehrlich et al. 2012). The structural and functional maturation of amygdala neurons may underlie a variety of developmental changes to emotional behavior occurring between P7 and P28, which are outlined in Table 1 (for review, see King et al. 2013), including conditioned avoidance (Sullivan et al. 2000), fear-potentiated startle (Hunt et al. 1994; Richardson et al. 2000), trace conditioning (Moye and Rudy 1987), and extinction (Kim and Richardson 2007). Our observations suggest that developmental changes in the amygdala extend from birth until adolescence, based on developmental milestones in the rat (Quinn 2005). More specifically, a P12 rat is in some ways comparable to a newborn human, while adolescence in rats is thought to begin around P28 and adulthood at P60.

Somatic development

The most basic metrics of morphological development we examined were somatic volume and surface area. Values for both measures increased dramatically from P7 to P28, with soma volume nearly doubling in this window, and remaining stable between P28 and P60. Our measurements of adult soma size are larger than those from a previous report in rat amygdala (Chareyron et al. 2011); the different estimates are likely due to technical differences, potentially due to methodology for calculating soma size or bias introduced by visual selection for patch clamp recording. Nevertheless, we have shown that in rat BLA principal neurons the most drastic increase in soma size parallels the major period of dendritic outgrowth suggesting the soma may enlarge specifically during a period of dendritic outgrowth, potentially to produce proteins or support the assembly of microtubules for dendritic growth (Baas and Lin 2011). Pyramidal cells in layer V of the prefrontal cortex exhibit somatic enlargement with the same developmental trajectory as BLA principal neurons (Zhang 2004), suggesting neuron maturation occurs in parallel in these regions.

Dendritic morphology

Our data suggest almost all growth of the dendritic arbor of BLA principal neurons occurs by P28, with a large proportion occurring between P7 and P21. While the aggregate length of dendritic material reaches the mature value around P21, Sholl analyses suggest the dendritic arbor is still remodeled beyond this time-point. Dendrites retracted from P21 to P28, with an increase in dendritic material within 200 μm of the soma and a decrease at more distal regions. On the other hand, from P28 to P60 dendrites extended farther from the soma, with a loss of dendritic material within 140 μm of the soma and an increase at more distal regions. We also used a Sholl analysis to compare the distribution of branch points throughout development. Interestingly, the proportion of dendritic length for each branch order was comparable across ages, suggesting there is an optimal distribution of branch points in the dendritic arbor that is maintained through development. The total number of branch points was consistent at every age, as was the number of primary dendrites. Our Sholl analysis further revealed a shift of branch points

more distally with age. While P7 neurons have over half of their dendritic branch points within 40 μm of the soma, for P60 the proportion is below one-quarter. On the other hand, at P60 nearly one-sixth of branch points are found between 120 and 160 μm from the soma, a much greater proportion than at any earlier time-point. The net effect of these changes is that the critical value is found gradually farther from the soma until P28. Maturation of the dendritic arbor is dependent on the excitatory actions of GABA early in development, and loss of excitatory GABA in development severely limits dendritic arborization and complexity (Cancedda et al. 2007). We have reported that GABAergic transmission onto BLA principal neurons is excitatory at P7 but switches to inhibitory by P14, suggesting the first two postnatal weeks represent a critical period for dendrite maturation (Ehrlich et al. 2013). Furthermore, activation of $GABA_B$ receptors early in development has been shown to promote dendrite outgrowth, and we have previously demonstrated large $GABA_B$ responses in P7 and P14 BLA principal neurons that diminish by P21, when dendrite expansion ends (Bony et al. 2013; Ehrlich et al. 2013).

The developmental trajectory of dendritic arbor morphology we report here is corroborated by previous studies in the BLA and developmental studies of pyramidal neurons in other brain regions. A previous study of BLA principal neurons in adult rats found a comparable spatial distribution of dendrites to our P60 time-point using a traditional Sholl analysis (Yajeya et al. 1997). A morphological analysis of developing layer V pyramidal neurons in somatosensory cortex by Romand and colleagues revealed a very similar growth pattern in the distribution of dendritic material, although their Sholl curves were notably broader, likely due to larger aggregate dendritic lengths (2,011). Stereological studies in the rat have also shown an increase in the volume of the rat BLA between P7 and P21, consistent with an expansion of dendritic arbors of BLA neurons during this period (Chareyron et al. 2012). Furthermore, a Golgi-Cox study of developing BLA neurons, which reported the area encompassed by the dendritic arbor, found a similar expansion during the first few postnatal weeks, albeit with substantially smaller arbors (Escobar and Salas 1993). Notably, previous Golgi-Cox studies of adult BLA neurons have estimated the aggregate dendritic length between 300 and 2,000 μm (Tosevski et al. 2002; Johnson et al. 2009; Pillai et al. 2012; Torres-Garcia et al. 2012), which differs greatly from our measurement of $\sim$ 6,400 μm at P60. We argue that the Golgi-Cox technique provides underestimates of dendritic length, possibly by selectively sampling smaller neurons or staining only proximal dendritic segments. However, it is possible we are overestimating the dendritic length due to bias in the visual selection of neurons for patch clamp. It is important to note that our slice thickness was slightly smaller at P7 and P14 (300 μm) than at later ages (350 μm) due to technical considerations, which could negatively bias the measurements of aggregate dendritic length in early tissue. However, the dendritic arbor of neurons at the early time-points has a much smaller diameter than at older time-points (< 300 μm at P7 vs > 500 μm at P60). Therefore, assuming the distribution of dendritic material is roughly spherical on average, we likely sampled a larger proportion of the overall dendritic arbor of P7 and P14 neurons, despite the smaller slice thickness. Interestingly, while BLA principal neurons exhibit an increase in aggregate dendritic length of more than threefold from P7 to P28, layer V pyramidal cells in the prefrontal cortex exhibit only a 2-fold increase in apical dendrite length during the same window (Zhang 2004). These results suggest BLA principal neurons are relatively less developed at P7 than those in prefrontal cortex.

The growth of the dendritic arbor in both quantity and complexity has substantial implications for neuronal physiology, particularly passive electrical properties. The increase in neuronal surface area across the first postnatal month undoubtedly contributes to the concurrent, nearly tenfold decrease in input resistance and threefold decrease in membrane time constant we previously reported in this cell population (Ehrlich et al. 2012). Furthermore, multicompartment modeling has revealed that expansion of the dendritic arbor can promote the expression of doublets of action potentials, driven by depolarization of the soma due to a dendritic spike (Mainen and Sejnowski 1996). In our hands, the expansion of the dendritic arbor of BLA principal neurons during the first postnatal month reported here does in fact correspond with the emergence of doublets (Ehrlich et al. 2012). In addition, expansion of the dendritic arbor has the potential to effectively increase the diversity of presynaptic partners or sensory modalities of input for a BLA principal neuron, due to the topographical organization of sensory input to the BLA (McDonald 1998). Interestingly, these inputs also undergo developmental change; tract-tracing studies have demonstrated thalamic afferents are present in the BLA at P7 and remain relatively unchanged with age, while cortical afferents continue to mature throughout the first postnatal month (Bouwmeester et al. 2002). It will be critical for future studies to address the sensitivity of this developmental trajectory to experience, considering the well-documented effects of stressors on the dendritic arborization of principal neurons in the adult BLA (Roozendaal et al. 2009; Padival et al. 2013) and in the case of autism spectrum disorders and Fragile X syndrome (Kaufmann and Moser 2000; Beckel-Mitchener and Greenough 2004; Puram et al. 2011).

Dendritic spine emergence

As the dendritic arbor expands throughout the first postnatal month, BLA principal neurons come to express many more dendritic spines. We observed a progressive increase in the density of dendritic spines between P7 and P28, by which time spines are as dense as in adulthood ($\sim$ 1.2 spines/μm at P60). Given the concurrent increase in aggregate dendritic length, BLA principal neurons have approximately 17 times as many spines at P60 as at P7. Comparable studies examining the development of dendritic spines in other brain regions have reported similar spine densities and developmental trajectories. For example, the spine density of layer V neurons in somatosensory cortex stabilizes around P21 at $\sim$ 0.6 spines/μm (Romand et al. 2011). Previous measurements of spine density in the BLA have yielded values slightly lower than ours, $\sim$ 0.7 spines/μm in late-adolescence (Torres-Garcia et al. 2012). This discrepancy may be because this study utilized the Golgi-Cox staining method, which, as discussed above, may be biased towards proximal dendrites. It is important to consider that our analysis counted and grouped all protrusions, including filopodia, and we have therefore likely overestimated the number of functional synaptic compartments. Furthermore, the developmental trajectories portrayed here do not account for possible age-dependent variation in the proportion of dendritic spines of various morphology. Finally, our analysis does not address the distribution of spine density with respect to distance from the soma or dendritic branch order. However, previous studies have demonstrated that the more proximal dendrites (< 90 μm from the soma) of glutamatergic projection neurons are typically spine sparse, spine density peaks $\sim$ 100 μm from the soma, and then a modest decrease in spine density is seen at more distal dendrites (Ballesteros-Yáñez et al. 2006; Elston and DeFelipe 2002). Future studies should examine the relationship between spine density and branch order throughout morphological development.

Interestingly, previous studies of synapse formation in the developing BLA, measured by synaptophysin staining, show the number of presynaptic terminals reaches a peak at P14 (Morys et al. 1998), while our data show that dendritic spines reach about half their mature density at this age. Although synaptophysin is not specific for afferents of principal neurons or those targeting dendritic spines, this mismatch in synaptophysin and spine development suggests during the first few postnatal weeks glutamatergic presynaptic terminals may form synapses with dendritic shafts or release transmitter without direct synaptic contact. The emergence of dendritic spines corresponds with the age when glutamate removal from synapses switches from primarily diffusion based to uptake dependent (Thomas et al. 2011). The early peak of synaptophysin expression may indicate an increase in glutamatergic transmission that could trigger the outgrowth of dendritic spines (Calabrese et al. 2006). In support of this notion, tract-tracing studies have shown that putative glutamatergic inputs to the BLA mature between P7 and P13 (Bouwmeester et al. 2002) and stabilize by P25, before undergoing pruning in late adolescence (Cressman et al. 2010). Dopaminergic and noradrenergic inputs to the BLA, which largely target spine shafts and heads on distal dendrites (Muller et al. 2009; Muly et al. 2009; Zhang et al. 2013), become more dense between P14 and P20 (Brummelte and Teuchert-Noodt 2006). Our own previous work demonstrates the presence of stimulation-evoked and spontaneous glutamatergic transmission onto BLA principal neurons as early as P7 (Ehrlich et al. 2013), when very few spines are present.

The emergence of dendritic spines in BLA principal neurons has numerous potential implications for neurotransmission in the amygdala. Glutamatergic afferents to the BLA are thought to provide representations for sensory stimuli that are critical to amygdala function, including noxious and neutral stimuli that undergo plasticity during associative fear learning (Rodrigues et al. 2004; Maren 2005; Pape and Pare 2010). Our results suggest BLA principal neurons have an order of magnitude more sites to potentially receive glutamatergic afferents by P60 than at P7. Dendritic spines also provide a means of compartmentalization of biochemical and electrical signals related to neurotransmission (Shepherd 1996; Lee et al. 2012), meaning the lack of spines early in development should impact the specificity of synaptic plasticity. Coincidentally, during the same window when spines emerge and reach mature numbers, there is increased abundance in BLA synaptic terminals of zinc, which promotes long-term potentiation of glutamatergic synapses in the BLA (Mizukawa et al. 1989; Li et al. 2011). Interestingly, juvenile mice exhibit generalization of conditioned fear, which could be related to poor specificity of synaptic plasticity (Ito et al. 2009). During infancy, rats also exhibit deficits to fear learning, and many forms of associative emotional learning emerge during the first few postnatal weeks (for review, see King et al. 2013). Perhaps most interesting is the observation that the amygdala is activated by odor-shock pairing after but not before P10, corresponding with the emergence of aversive conditioning and a change in amygdala synaptic plasticity (Sullivan et al. 2000; Thompson et al. 2008), precisely when dendritic spines begin to emerge.

Here we have shown that the morphology of BLA principal neurons matures profoundly across the first two postnatal months and discussed these changes in the context of concurrent, substantial changes to neuronal physiology, animal behavior, and synaptic plasticity. Together,

these findings clearly illustrate that the first postnatal month, a previously defined critical period of rodent development, includes morphological changes in brain regions that process emotion. Developmental milestones in emotional behavior suggest the maturation of dendritic branching and spine emergence of amygdala neurons observed here, as well as the physiological changes we previously reported, contribute to the early emergence of innate fear-related behavior and the improved ability to form associative memories and integrate increasingly complex stimuli with age. Future studies should address how genetic and environmental factors, such as stress or exposure to teratogens, can alter the developmental trajectory of neurons in the BLA. It will be important to consider the findings of this study when developing models for the etiology of developmental psychiatric disorders.

Acknowledgments The authors would like to thank Prof. Todd Preuss for resources for the analysis of neuron morphology and the Emory University Institute for Quantitative Theory and Methods for assistance with statistical analyses. This work was funded by the following grants from the National Institutes of Health: MH 069852 to D.G.R., base grant RR 00165 to the Yerkes National Primate Research center, and MH 090729 to D.E.E.

Conflict of interest The authors would like to declare no conflicts of interest.

Reference

Adolphs R, Baron-Cohen S, Tranel D (2002) Impaired recognition of social emotions following amygdala damage. J Cogn Neurosci 14(8):1264–1274

Baas PW, Lin S (2011) Hooks and comets: the story of microtubule polarity orientation in the neuron. Dev Neurobiol 71(6):403–418

Ballesteros-Yáñez I, Benavides-Piccione R, Elston GN, Yuste R, DeFelipe J (2006) Density and morphology of dendritic spines in mouse neocortex. Neuroscience 138(2):403–409

Barnet RC, Hunt PS (2005) Trace and long-delay fear conditioning in the developing rat. Learn Behav 33:437–443

Barnet RC, Hunt PS (2006) The expression of fear-potentiated startle during development: integration of learning and response systems. Behav Neurosci 120:861–872

Beckel-Mitchener A, Greenough WT (2004) Correlates across the structural, functional, and molecular phenotypes of fragile X syndrome. Ment Retard Dev D R 10(1):53–59

Berdel B, Moryś J (2000) Expression of calbindin-D28 k and parvalbumin during development of rat's basolateral amygdaloid complex. Int J Dev Neurosci 18(6):501–513

Bony G, Szczurkowska J, Tamagno I, Shelly M, Contestabile A, Cancedda L (2013) Non-hyperpolarizing GABAB receptor activation regulates neuronal migration and neurite growth and specification by cAMP/LKB1. Nat Commun 4:1800

Bouwmeester H, Smits K, Van Ree JM (2002) Neonatal development of projections to the basolateral amygdala from prefrontal and thalamic structures in rat. J Comp Neurol 450(3):241–255

Brummelte S, Teuchert-Noodt G (2006) Postnatal development of dopamine innervation in the amygdala and the entorhinal cortex of the gerbil (Meriones unguiculatus). Brain Res 1125(1): 9–16

Calabrese B, Wilson MS, Halpain S (2006) Development and regulation of dendritic spine synapses. Physiol (Bethesda) 21:38–47

Camp LL, Rudy JW (1988) Changes in the categorization of appetitive and aversive events during postnatal development of the rat. Dev Psychobiol 21:25–42

Campbell BA, Ampuero MX (1985) Dissociation of autonomic and behavioral components of conditioned fear during development in the rat. Behav Neurosci 99:1089–1102

Cancedda L, Fiumelli H, Chen K, Poo M (2007) Excitatory GABA action is essential for morphological maturation of cortical neurons in vivo. J Neurosci 27(19):5224

Chareyron LJ, Banta Lavenex P, Amaral DG, Lavenex P (2011) Stereological analysis of the rat and monkey amygdala. J Comp Neurol 519(16):3218–3239

Chareyron LJ, Banta Lavenex P, Lavenex P (2012) Postnatal development of the amygdala: a stereological study in rats. J Comp Neurol 520(16):3745–3763

Cressman VL, Balaban J, Steinfeld S, Shemyakin A, Graham P, Parisot N, Moore H (2010) Prefrontal cortical inputs to the basal amygdala undergo pruning during late adolescence in the rat. J Comp Neurol 518(14):2693–2709

Davis M, Walker DL, Myers KM (2003) Role of the amygdala in fear extinction measured with potentiated startle. Ann NY Acad Sci 985:218–232

Ehrlich DE, Ryan SJ, Rainnie DG (2012) Postnatal development of electrophysiological properties of principal neurons in the rat basolateral amygdala. J Physiol 590(19):4819–4838

Ehrlich DE, Ryan SJ, Hazra R, Guo JD, Rainnie DG (2013) Postnatal maturation of GABAergic transmission in the rat basolateral amygdala. J Neurophysiol 110(4):926–941

Elston GN, DeFelipe J (2002) Spine distribution in cortical pyramidal cells: a common organizational principle across species. Prog Brain Res 136:109–133

Escobar C, Salas M (1993) Neonatal undernutrition and amygdaloid nuclear complex development: an experimental study in the rat. Exp Neurol 122(2):311–318

Gleich O, Strutz J (2002) Age dependent changes in the medial nucleus of the trapezoid body in gerbils. Hearing Res 164(1–2):166–178

Hubbard DT, Blanchard DC, Yang M, Markham CM, Gervacio A, Chun-I L, Blanchard RJ (2004) Development of defensive behavior and conditioning to cat odor in the rat. Physiol Behav 80(4):525–530

Hunt PS (1999) A further investigation of the developmental emergence of fear-potentiated startle in rats. Devel Psychobiol 34:281–291

Hunt PS, Richardson R, Campbell BA (1994) Delayed development of fear-potentiated startle in rats. Behav Neurosci 108(1):69–80

Hunt PS, Hess MF, Campbell BA (1998) Inhibition of the expression of conditioned cardiac responses in the developing rat. Devel Psychobiol 33(3):221–233

Ito W, Pan BX, Yang C, Thakur S, Morozov A (2009) Enhanced generalization of auditory conditioned fear in juvenile mice. Learn Mem 16(3):187–192

Johnson SA, Wang JF, Sun X, McEwen BS, Chattarji S, Young LT (2009) Lithium treatment prevents stress-induced dendritic remodeling in the rodent amygdala. Neuroscience 163(1):34–39

Kaufmann WE, Moser HW (2000) Dendritic anomalies in disorders associated with mental retardation. Cereb Cortex 10(10):981–991

Kim JH, Richardson R (2007) A developmental dissociation in reinstatement of an extinguished fear response in rats. Neurobiol Learn Mem 88(1):48–57

Kim JH, Richardson R (2008) The effect of temporary amygdala inactivation on extinction and reextinction of fear in the

developing rat: unlearning as a potential mechanism for extinction early in development. J Neurosci 28(6):1282–1290
Kim-Cohen J, Caspi A, Moffitt TE, Harrington HL, Milne BJ, Poulton R (2003) Prior juvenile diagnoses in adults with mental disorder: developmental follow-back of a prospective-longitudinal cohort. Arch Gen Psych 60(7):709–717
King EC, Pattwell SS, Glatt CE, Lee FS (2013) Sensitive periods in fear learning and memory. Stress 17(1):13–21
Koob GF, Volkow ND (2010) Neurocircuitry of addiction. Neuropsychopharm 35(1):217–238
Langton JM, Kim JH, Nicholas J, Richardson R (2007) The effect of the NMDA receptor antagonist MK-801 on the acquisition and extinction of learned fear in the developing rat. Learn Mem 14:665–668
LeDoux JE (2007) The amygdala. Curr Biol 17(20):R868–R874
Lee KF, Soares C, Béïque JC (2012) Examining form and function of dendritic spines. Neural Plast 2012:704103
Li C, Dabrowska J, Hazra R, Rainnie DG (2011) Synergistic activation of dopamine D1 and TrkB receptors mediate gain control of synaptic plasticity in the basolateral amygdala. PLoS ONE 6(10):e26065
Liao CC, Lee LJ (2012) Evidence for structural and functional changes of subplate neurons in developing rat barrel cortex. Brain Struct Funct 217(2):275–292
Mainen ZF, Sejnowski TJ (1996) Influence of dendritic structure on firing pattern in model neocortical neurons. Nature 382(6589):363–366
Maren S (2005) Synaptic mechanisms of associative memory in the amygdala. Neuron 47(6):783–786
McDonald AJ (1998) Cortical pathways to the mammalian amygdala. Prog Neurobiol 55(3):257–332
McEwen BS (2003) Early life influences on life-long patterns of behavior and health. Ment Retard Dev D R 9(3):149–154
Mizukawa K, Tseng IM, Otsuka N (1989) Quantitative electron microscopic analysis of postnatal development of zinc-positive nerve endings in the rat amygdala using timm's sulphide silver technique. Brain Res Dev Brain Res 50(2):197–203
Monteiro RA, Henrique RM, Rocha E, Marini-Abreu MM, Oliveira MH, Silva MW (1998) Age-related changes in the volume of somata and organelles of cerebellar granule cells. Neurobiol Aging 19(4):325–332
Monteiro RA, Henrique RM, Oliveira MH, Silva MW, Rocha E (2005) Postnatal cerebellar granule cells of the white rat (rattus norvegicus): a quantitative study, using design-based stereology. Ann Anat 187(2):161–173
Moriceau S, Roth TL, Okotoghaide T, Sullivan RM (2004) Corticosterone controls the developmental emergence of fear and amygdala function to predator odors in infant rat pups. Int J Dev Neurosci 22:415–422
Moryś J, Berdel B, Kowiański P, Dziewiatkowski J (1998) The pattern of synaptophysin changes during the maturation of the amygdaloid body and hippocampal hilus in the rat. Folia Neuropathol 36(1):15–23
Moye TB, Rudy JW (1987) Ontogenesis of trace conditioning in young rats: dissociation of associative and memory processes. Dev Psychobiol 20(4):405–414
Muller JF, Mascagni F, McDonald AJ (2009) Dopaminergic innervation of pyramidal cells in the rat basolateral amygdala. Brain Struct Funct 213(3):275–288
Muly EC, Senyuz M, Khan ZU, Guo JD, Hazra R, Rainnie DG (2009) Distribution of D1 and D5 dopamine receptors in the primate and rat basolateral amygdala. Brain Struct Funct 213(4–5): 375–393
Padival MA, Blume SR, Rosenkranz JA (2013) Repeated restraint stress exerts different impact on structure of neurons in the lateral and basal nuclei of the amygdala. Neurosci 246:230–242
Pape HC, Pare D (2010) Plastic synaptic networks of the amygdala for the acquisition, expression, and extinction of conditioned fear. Physiol Rev 90(2):419
Pattwell SS, Bath KG, Casey BJ, Ninan I, Lee FS (2011) Selective early-acquired fear memories undergo temporary suppression during adolescence. Proc Natl Acad Sci USA 108(3):1182–1187
Pattwell SS, Duhoux S, Hartley CA, Johnson DC, Jing D, Elliott MD, Ruberry EJ, Powers A, Mehta N, Yang RR, Soliman F, Glatt CE, Casey BJ, Ninan I, Lee FS (2012) Altered fear learning across development in both mouse and human. Proc Natl Acad Sci USA 109(40):16318–16323
Paxinos G, Watson C (1997) The rat brain in stereotaxic coordinates, 3rd edn. Academic Press, San Diego
Pillai AG, de Jong D, Kanatsou S, Krugers H, Knapman A, Heinzmann JM, Holsboer F, Landgraf R, Joëls M, Touma C (2012) Dendritic morphology of hippocampal and amygdalar neurons in adolescent mice is resilient to genetic differences in stress reactivity. PLoS ONE 7(6):e38971
Pine DS, Cohen P, Gurley D, Brook J, Ma Y (1998) The risk for early-adulthood anxiety and depressive disorders in adolescents with anxiety and depressive disorders. Arch Gen Psychiatry 55(1):56–64
Puram SV, Kim AH, Ikeuchi Y, Wilson-Grady JT, Merdes A, Gygi SP, Bonni A (2011) A CaMKIIβ signaling pathway at the centrosome regulates dendrite patterning in the brain. Nat Neurosci 14(8):973–983
Quinn R (2005) Comparing rat's to human's age: How old is my rat in people years? Nutrition 21(6):775–777
Raineki C, De Souza MA, Szawka RE, Lutz ML, De Vasconcellos LF, Sanvitto GL, Izquierdo I, Bevilaqua LR, Cammarota M, Lucion AB (2009) Neonatal handling and the maternal odor preference in rat pups: involvement of monoamines and cyclic AMP response element-binding protein pathway in the olfactory bulb. Neuroscience 159(1):31–38
Rainnie DG (1999) Serotonergic modulation of neurotransmission in the rat basolateral amygdala. J Neurophysiol 82(1):69-85
Rainnie DG, Bergeron R, Sajdyk TJ, Patil M, Gehlert DR, Shekhar A (2004) Corticotrophin releasing factor-induced synaptic plasticity in the amygdala translates stress into emotional disorders. J Neurosci 24(14):3471–3479
Rainnie DG, Mania I, Mascagni F, McDonald AJ (2006) Physiological and morphological characterization of parvalbumin-containing interneurons in the rat basolateral amygdala. J Comp Neurol 498(1):142–161
Richardson R, Paxinos G, Lee J (2000) The ontogeny of conditioned odor potentiation of startle. Behav Neurosci 114(6):1167–1173
Rodrigues SM, Schafe GE, LeDoux JE (2004) Molecular mechanisms underlying emotional learning and memory in the lateral amygdala. Neuron 44(1):75–91
Romand S, Wang Y, Toledo-Rodriguez M, Markram H (2011) Morphological development of thick-tufted layer v pyramidal cells in the rat somatosensory cortex. Front Neuroanat 5:5
Roozendaal B, McEwen BS, Chattarji S (2009) Stress, memory and the amygdala. Nat Rev Neurosci 10(6):423–433
Rubinow MJ, Drogos LL, Juraska JM (2009) Age-related dendritic hypertrophy and sexual dimorphism in rat basolateral amygdala. Neurobiol Aging 30(1):137–146
Rudy JW (1993) Contextual conditioning and auditory cue conditioning dissociate during development. Behav Neurosci 107(5):887–891
Ryan SJ, Ehrlich DE, Jasnow AM, Daftary S, Madsen TE, Rainnie DG (2012) Spike-timing precision and neuronal synchrony are enhanced by an interaction between synaptic inhibition and membrane oscillations in the amygdala. PLoS ONE 7(4):e35320
Shekhar A, Truitt W, Rainnie DG, Sajdyk T (2005) Role of stress, corticotrophin releasing factor (CRF) and amygdala plasticity in chronic anxiety. Stress 8(4):209–219

Shepherd GM (1996) The dendritic spine: a multifunctional integrative unit. J Neurophysiol 75(6):2197–2210

Steinberg L (2005) Cognitive and affective development in adolescence. Trends Cogn Sci 9(2):69–74

Stuber GD, Sparta DR, Stamatakis AM, van Leeuwen WA, Hardjoprajitno JE, Cho S, Tye KM, Kempadoo KA, Zhang F, Deisseroth K, Bonci A (2011) Excitatory transmission from the amygdala to nucleus accumbens facilitates reward seeking. Nature 475(7356):377–380

Sullivan RM, Landers M, Yeaman B, Wilson DA (2000) Good memories of bad events in infancy. Nature 407(6800):38–39

Takahashi LK (1992) Ontogeny of behavioral inhibition induced by unfamiliar adult male conspecifics in preweanling rats. Physiol Behav 52:493–498

Thomas CG, Tian H, Diamond JS (2011) The relative roles of diffusion and uptake in clearing synaptically released glutamate change during early postnatal development. J Neurosci 31(12):4743–4754

Thompson JV, Sullivan RM, Wilson DA (2008) Developmental emergence of fear learning corresponds with changes in amygdala synaptic plasticity. Neuroscience 1200:58–65

Torres-García ME, Solis O, Patricio A, Rodríguez-Moreno A, Camacho-Abrego I, Limón ID, Flores G (2012) Dendritic morphology changes in neurons from the prefrontal cortex, hippocampus and nucleus accumbens in rats after lesion of the thalamic reticular nucleus. Neuroscience 223:429–438

Tosevski J, Malikovic A, Mojsilovic-Petrovic J, Lackovic V, Peulic M, Sazdanovic P, Alexopulos C (2002) Types of neurons and some dendritic patterns of basolateral amygdala in humans: a golgi study. Ann Anat 184(1):93–103

Truitt WA, Sajdyk TJ, Dietrich AD, Oberlin B, McDougle CJ, Shekhar A (2007) From anxiety to autism : spectrum of abnormal social behaviors modeled by progressive disruption of inhibitory neuronal function in the basolateral amygdala in Wistar rats. Psychopharmacology 191(1):107–118

Vidal L, Ruíz C, Villena A, Díaz F, Pérez de Vargas I (2004) Quantitative age-related changes in dorsal lateral geniculate nucleus relay neurons of the rat. Neurosci Res 48(4):387–396

Wiedenmayer CP, Barr GA (2001) Developmental changes in responsivity to threat are stimulus-specific in rats. Dev Psychobiol 39(1):1–7

Yajeya J, de la Fuente Juan A, Merchan MA, Riolobos AS, Heredia M, Criado JM (1997) Cholinergic responses of morphologically and electrophysiologically characterized neurons of the basolateral complex in rat amygdala slices. Neuroscience 78(3):731–743

Zhang ZW (2004) Maturation of layer V pyramidal neurons in the rat prefrontal cortex: intrinsic properties and synaptic function. J Neurophysiol 91(3):1171–1182

Zhang J, Muller JF, McDonald AJ (2013) Noradrenergic innervation of pyramidal cells in the rat basolateral amygdala. Neuroscience 228:395–408